






Original Research

Sodium Alginate Microgel-Wrapped Primary Human Peritoneal Mesothelial Cells for the Treatment of Peritoneal Fibrosis Caused by Dialysis via the POSTN/NF- κ B/CXCL8 Pathway

Shuqing Ma^{1,2,†}, Chunyan Qiu^{2,†}, Jue Zhang², Luhui Wang², Yaozhe Ying³, Ke Zhang², Xiao Yang⁴, Changcan Shi⁴, Yunting Wang⁵, Chenfei Zheng⁶, Zhe Lin⁶, Chaosheng Chen⁶, Yongheng Bai¹, Yangping Shentu⁷, Chunwu Zhang⁸, Ying Zhou^{6,8,*}

¹Zhejiang Key Laboratory of Intelligent Cancer Biomarker Discovery and Translation, The First Affiliated Hospital of Wenzhou Medical University, 325035 Wenzhou, Zhejiang, China

²The First School of Medicine and the School of Information and Engineering, Wenzhou Medical University, 325035 Wenzhou, Zhejiang, China

³Department of Clinical Nutrition, Wenzhou People's Hospital & Wenzhou Women's and Children's Hospital, 325035 Wenzhou, Zhejiang, China

⁴Wenzhou Key Laboratory of Biophysics, Wenzhou Institute, University of Chinese Academy of Sciences, 325035 Wenzhou, Zhejiang, China

⁵Department of Pharmacological and Pharmaceutical Sciences, College of Pharmacy, University of Houston, Houston, TX 77001, USA

⁶Department of Nephrology, The First Affiliated Hospital of Wenzhou Medical University, 325035 Wenzhou, Zhejiang, China

⁷Department of Pathology, The First Affiliated Hospital of Wenzhou Medical University, 325035 Wenzhou, Zhejiang, China

⁸Geriatrics Center, The First Affiliated Hospital of Wenzhou Medical University, 325035 Wenzhou, Zhejiang, China

*Correspondence: zhouying610@163.com (Ying Zhou)

†These authors contributed equally.

Academic Editor: Esteban C. Gabazza

Submitted: 7 August 2025 Revised: 1 November 2025 Accepted: 13 November 2025 Published: 27 November 2025

Abstract

Background: Peritoneal fibrosis is a significant complication arising from long-term peritoneal dialysis (PD), primarily due to the loss of peritoneal mesothelial cells (PMCs). Recent studies have implicated periostin (POSTN) in the progression of various fibrotic diseases; however, its specific role in PD-induced peritoneal fibrosis remains unclear. Sodium alginate (SA) microgels have emerged as promising carriers for cell encapsulation in tissue engineering and regenerative medicine. This study investigated the therapeutic potential of PMCs encapsulated in SA microgels (SA/PMC) for reducing PD-induced peritoneal fibrosis, with a focus on the modulation by the periostin/nuclear factor kappa-B (NF- κ B)/CXCL8 signaling pathway. **Methods:** Primary human peritoneal mesothelial cells (PHPMCs) were isolated from the PD effluent of patients. The effect of SA encapsulation on PMCs proliferation was evaluated using a Cell Counting Kit 8 (CCK-8) assay. The expression levels of POSTN, NF- κ B p65, and CXCL8, as well as fibrosis markers, including α -smooth muscle actin (α -SMA), collagen I, transforming growth factor- β (TGF- β), and fibronectin, were evaluated in patients undergoing PD and a PD mouse model. **Results:** Patients undergoing PD for 1 year exhibited elevated levels of POSTN, NF- κ B p65, CXCL8, and fibrosis markers compared with those undergoing PD for 1 week. **Conclusions:** Consistent results from *in vivo* and *in vitro* models demonstrated that PD and hyperglycemic conditions upregulated the expression of POSTN, NF- κ B p65, CXCL8, and profibrotic markers, leading to peritoneal thickening and fibrotic progression. Treatment with SA/PMC microgels ameliorated these effects. By modulating the POSTN/NF- κ B/CXCL8 pathway and enhancing PMCs survival, SA/PMC microgels may have therapeutic potential in mitigating peritoneal fibrosis in PD patients.

Keywords: sodium alginate; microgels; periostin; peritoneal fibrosis; peritoneal dialysis

1. Introduction

Peritoneal dialysis (PD) is widely utilized as a primary renal replacement therapy, benefiting an increasing number of patients with chronic kidney disease (CKD) [1]. However, peritoneal fibrosis remains a significant and prevalent complication in patients undergoing long-term PD, severely compromising therapeutic effectiveness and quality of life [2]. Clinical observations indicate that approximately 50–80% of patients who undergo PD for more than two years develop varying degrees of peritoneal fibrosis, ultimately leading to technique failure and increased morbidity [3].

A critical factor underlying PD-associated peritoneal fibrosis is the continuous damage and loss of peritoneal mesothelial cells (PMCs). These cells play a crucial role in maintaining peritoneal integrity and function, including anti-inflammatory effects, fibrinolysis, and tissue repair [4]. During PD, repetitive mechanical stress and continuous exposure to hypertonic, glucose-based dialysis solutions induce injury and epithelial-mesenchymal transition (EMT). This is characterized by significant increases in the expression of fibrosis-related proteins such as α -smooth muscle actin (α -SMA), collagen I, fibronectin (FN), and transforming growth factor- β 1 (TGF- β 1) [5–7]. Despite concerted



efforts, current therapies targeting PD-related peritoneal fibrosis remain insufficient, highlighting the urgent need for novel and more effective treatment strategies.

Mesothelial cell transplantation represents a promising therapeutic approach for peritoneal fibrosis, demonstrating potential in the regeneration of damaged peritoneal tissues [8,9]. However, conventional PMC transplantation faces several significant challenges, including limited cell viability, rapid cell loss, and poor targeted delivery within the peritoneal cavity, thus restricting clinical applicability. To overcome these limitations, recent advances in biomaterial science have shown considerable promise, in particular the use of sodium alginate (SA)-based microencapsulation technologies [10,11]. SA is a naturally derived biocompatible and biodegradable polysaccharide that is increasingly utilized in cell transplantation due to its protective and proliferation-promoting properties [12].

Sodium alginate, a natural polysaccharide from brown algae, is highly valued in biomedical engineering for its excellent biocompatibility and biodegradability. Research shows that in animal models, alginate microcapsules act as a protective shield, effectively isolating transplanted islet cells from immune rejection and enabling them to maintain long-term blood sugar control [13]. A clinical study led by Anil Dhawan's team [14] further demonstrated the safety and feasibility of this approach. They successfully used alginate microcapsules to transplant human liver cells into eight children with acute liver failure. In spinal cord injury treatment, scientists are using advanced 3D printing to create structured alginate hydrogel scaffolds. These scaffolds not only provide physical support but also actively boost the function of the body's own neural stem cells, encouraging repair [15]. Together, these advances highlight the promising potential of sodium alginate as a cell carrier for treating a range of diseases through regenerative medicine.

This study seeks to elucidate the therapeutic efficacy and mechanistic basis of PMCs encapsulated in SA (SA/PMC) in mitigating peritoneal fibrosis induced by PD. We employed high-glucose-induced *in vitro* EMT models and *in vivo* murine models of peritoneal fibrosis to evaluate targeting efficiency, cell viability, inflammatory responses, and the expression of fibrosis-related proteins. The findings of this study have significant potential for developing a novel, cell-based therapeutic strategy that addresses the limitations of conventional PMC transplantation. This should ultimately improve clinical outcomes, extend peritoneal functional lifespan, and enhance the prognosis and quality of life for PD patients.

2. Materials and Methods

2.1 Preparation of SA Microgels

SA microgels were prepared following established protocols [16,17]. A calcium-EDTA (Ca-EDTA) complex was formulated by combining calcium chloride and disodium EDTA in a 1:1 molar ratio, and adjusting the pH to

7.4 using sodium hydroxide. The aqueous phase consisted of 1% SA (MACKLIN, Shanghai, China) and 50 mM Ca-EDTA dissolved in distilled water, followed by filtration through a 0.22 μm syringe filter (FMC201030, JETBIOFIL, Guangzhou, China). For cell-laden microgels, primary human PMCs (PHPMCs) at a density of 5×10^6 cells/mL were suspended in the aqueous phase. Two milliliters of droplet generation oil (FluidicLab, China) were filtered using a 0.22 μm syringe filter. All microfluidic encapsulation devices were sterilized with 75% ethanol and exposed to ultraviolet light overnight prior to use. The aqueous and oil phases were loaded into separate syringes and mounted on a laboratory syringe pump (LSP01-3A, LONGER, Tucson, AZ, USA), connected to a microfluidic chip (PDMS-FF-100B, FluidicLab, Shanghai, China) to ensure uniformity. Flow rates were maintained at 7 $\mu\text{L}/\text{min}$ for the aqueous phase and 35 $\mu\text{L}/\text{min}$ for the oil phase. The resultant gel was collected in culture medium for subsequent experiments. The encapsulation rate and release curve of sodium alginate microgel were determined by cell counting kit 8 (CCK-8) method.

2.2 Isolation and Culture of PHPMCs

The study protocol was approved by the Human Ethics Committee of Wenzhou Medical University (Acceptance number: KY2024-R179). The research adhered to Good Clinical Practice guidelines and followed the principles of the Declaration of Helsinki. PHPMCs were isolated from PD effluent of patients undergoing dialysis at the First Affiliated Hospital of Wenzhou Medical University. Inclusion criteria were: (1) absence of peritonitis during PD; (2) regular PD follow-up; (3) age between 40 and 60 years; (4) no malignant tumors; (5) no ascites; and (6) signed informed consent. No statistically significant disparities in age, gender, or educational background were observed across the participant cohorts ($p > 0.05$). PD effluent samples were collected after durations of 1 week (1W), 1 year (1Y), and 3 years (3Y) of PD ($n = 30$ per group). The surface of the PD fluid specimen bag was disinfected with 75% ethanol before sterile collection. Samples were aliquoted into 50 mL centrifuge tubes and centrifuged at $1000 \times g$ for 5 minutes at 4 $^{\circ}\text{C}$ to pellet the PHPMCs, with the supernatant discarded. Cells were resuspended in Dulbecco's Modified Eagle Medium/Nutrient Mixture F-12 (DMEM/F12) (Gibco, CA, USA) supplemented with 10% fetal bovine serum (FBS) and 1% penicillin-streptomycin, and cultured in dishes at 37 $^{\circ}\text{C}$ with 5% CO_2 . The medium was refreshed every 2–3 days to remove non-adherent cells. PHPMCs were characterized by immunofluorescence staining for cytokeratin 18 (CK18) and vimentin to confirm mesothelial origin. Upon reaching 80–90% confluence, cells were trypsinized with 0.25% trypsin-EDTA and reseeded for expansion.

In vitro models were established as follows: (1) the control (Con) group: PHPMCs cultured in DMEM/F12

medium for 96 h; (2) the high glucose (G) group: HPMCs cultured in DMEM/F12 medium supplemented with 60 mM glucose for 48 h to induce fibrosis, followed by replacement with normal DMEM/F12 medium for an additional 48 h; (3) the high glucose+SA (G+SA) group: PHPMCs cultured in high-glucose medium (60 mM) for 48 h, followed by co-culture with freshly prepared blank SA microgels for an additional 48 h (total 96 h); (4) the high glucose+SA/PMC (G+SA/PMC) group: PHPMCs cultured in high-glucose medium (60 mM) for 48 h, followed by co-culture with freshly prepared SA microgels encapsulating additional PHPMCs for another 48 h (total 96 h). Since PHPMCs are non-immortalized cells, they were used after 5–7 passages in both the *in vivo* and *in vitro* experiments.

2.3 Cell Proliferation Assay

Cell proliferation was assessed using the CCK-8 assay kit (Beyotime, Shanghai, China). PMCs were seeded in 96-well plates at a density of 5×10^3 cells per well and incubated at 37 °C with 5% CO₂ for 24 h to allow cell attachment. Subsequently, PMCs were co-incubated with SA and SA/PMC for 0, 24, 48, and 72 h. Following the designated incubation period, CCK-8 reagent was introduced into each well, subjected to gentle agitation, and further incubated for 1 h. Absorbance measurements (optical density, OD) were then conducted at 450 nm with a microplate reader (Thermo Fisher Scientific, Waltham, MA, USA). Each treatment group included at least three replicates, and the experiment was repeated three times. Cell proliferation was evaluated by comparing OD values across treatment groups at each time point. The PMCs cell lines were validated by STR profiling and tested negative for mycoplasma.

2.4 Model Mouse of PD

BALB/c nude mice (male, 8 weeks old) were provided by Charles River Laboratory Animal Technology Co., Ltd (Zhejiang, China). The mice were housed under standard laboratory conditions with a 12-h light/dark cycle, a temperature of 22 ± 1 °C, and *ad libitum* access to food and water. After one-week of acclimatization, the mice were randomly divided into five experimental groups (n = 3–5 per group): (1) the Con group received daily intraperitoneal (IP) administration of 10 mL/100 g of physiological saline for four consecutive weeks; (2) the PD group received IP injections of 10 mL/100 g of 4.25% glucose PD solution for four consecutive weeks; (3) the PD+SA group received IP injections of 10 mL/100 g of 4.25% glucose PD solution for four consecutive weeks, and SA microgels at the beginning of the second week; (4) the PD+PMC group received IP injections of 10 mL/100 g of 4.25% glucose PD solution for four consecutive weeks, and 5×10^6 PHPMCs at the beginning of the second week; (5) the PD+SA/PMC group received IP injections of 10 mL/100 g of 4.25% glucose PD solution for four consecutive weeks, and SA microspheres

encapsulating 5×10^6 PHPMCs at the beginning of the second week. The body weights of the mice were systematically monitored and documented both at baseline and at regular intervals during the experimental timeline.

To begin the terminal sampling procedure, mice were anesthetized with isoflurane vapor. Induction used 3–5% isoflurane in 100% oxygen (via nose cone or chamber), with a 1–3% concentration to maintain anesthesia. The depth of anesthesia was monitored every 2–3 minutes by checking foot-pinch reflexes and breathing rate. Throughout the process, the mice rested on a heating pad for thermoregulation, and eye lubricant was applied to prevent dryness. Since this was a terminal procedure, no post-operative pain management was needed. Once a surgical plane of anesthesia was achieved, we immediately performed cardiac blood collection, perfusion, or organ collection. For euthanasia, we used CO₂ inhalation ($\geq 99\%$ purity) at a fill rate of 30–70% of the chamber volume per minute without pre-charging. After the animals lost consciousness, CO₂ flow was continued for at least one minute. We then applied a secondary method, such as bilateral thoracotomy, exsanguination, or cervical dislocation, to ensure death. The blood, liver, heart, lungs, kidneys, and peritoneum of the mice were collected and preserved. Some portions of the tissues were immediately stored in a –80 °C freezer, while other portions were fixed in 4% paraformaldehyde.

2.5 Hematoxylin and Eosin (H&E) Staining

Harvested tissue specimens, including those from the liver, heart, lung, kidney, and peritoneum, underwent fixation in 4% paraformaldehyde for a duration of 48 h. Fixed tissues were dehydrated through a graded ethanol series, cleared in xylene, and embedded in paraffin. Paraffin-embedded tissues were sectioned at a thickness of 5 μ m using a microtome. Deparaffinization of tissue sections was carried out using xylene, followed by rehydration via a graded ethanol series, and culminating in immersion in distilled water. H&E staining was performed according to the instructions provided in the stain kit (Solarbio, Beijing, China). Sections were stained with hematoxylin for 5 minutes to visualize nuclei, then rinsed in running tap water. Eosin staining was performed for 2 minutes to stain the cytoplasm and extracellular matrix. Stained sections were dehydrated through increasing ethanol concentrations, cleared in xylene, and mounted with a coverslip using a synthetic resin. Images were captured using a Leica microscope (VT1000S, Shanghai, China). All experiments were repeated at least in triplicate.

2.6 MASSON Staining

MASSON staining was performed using a stain kit (Solarbio, Beijing, China) and following the manufacturer's protocol. Sections were immersed in Bouin solution overnight at 37 °C, then rinsed with running water until the yellow color disappeared. The sections were subse-

quently stained with aniline blue for 2 minutes and briefly rinsed with water. Mayer's hematoxylin was applied for 2 minutes, followed by a brief water rinse. The sections were differentiated in acidic ethanol for a few seconds and washed in running water for 10 minutes. Biebrich scarlet-acid fuchsin was applied for 10 minutes, the sections were then briefly rinsed with distilled water, followed by treatment with phosphomolybdic acid solution for about 10 minutes. Without washing, the aniline blue solution was directly applied for 5 minutes. The sections were subsequently treated with a weak acid solution for 2 minutes and quickly dehydrated in 95% ethanol. They were then dehydrated in absolute ethanol three times, each for 5–10 seconds, followed by clearing in xylene three times, each for 1–2 minutes. Finally, the sections were mounted with neutral resin, and images were captured using a Leica microscope. All experiments were repeated at least in triplicate.

2.7 Immunohistochemistry

Immunohistochemical analysis was conducted on tissue sections prepared from paraffin-embedded samples. The 4 μm slices were dewaxed in xylene and hydrated with graded ethanol solutions. Antigen retrieval was performed with citrate buffer, followed by treatment with 3% hydrogen peroxide. Subsequently, sections were blocked with goat serum for 1 h. The tissue sections were then incubated overnight at 4 °C with primary antibodies, including anti-periostin (POSTN) (1:100, DF6746, Affinity, Jiangsu, China), anti-nuclear factor kappa-B (NF- κ B) P65 (1:100, ab32536, Abcam, Cambridge, MA, USA), anti-phospho-NF- κ B P65 (p-P65, 1:100, AF2006, Affinity, China), anti-CXCL8 (1:100, DF6998, Affinity, China), anti- α -smooth muscle actin (α -SMA, 1:100, AF1032, Affinity, China), anti-collagen 1 (Col-1, 1:100, AF7001, Affinity, China), anti-transforming growth factor- β (TGF- β , 1:100, BF8012, Affinity, China), and anti-FN (1:100, AF5335, Affinity, China). After washing with phosphate buffered saline (PBS), HRP-labeled secondary antibodies were applied, followed by 3,3'-diaminobenzidine (DAB) chromogenic staining to visualize the bound antibodies, and hematoxylin counterstaining to highlight the nuclei. Images were captured using a Leica microscope, and all experiments were repeated in triplicate.

2.8 Immunofluorescence

Paraffin-embedded tissue sections (4 μm) were dewaxed in xylene and rehydrated through graded ethanol solutions. Antigen retrieval was performed using citrate buffer followed by 4% paraformaldehyde. Cell samples were washed three times with PBS and the cells then fixed with 4% paraformaldehyde. Both tissue and cell samples were permeabilized with 0.1% Triton X-100, and blocked with goat serum for 1 h. Samples were then incubated overnight at 4 °C with one or two primary antibodies from different sources. After washing with PBS, samples were

incubated at 37 °C for 1 h with corresponding secondary antibodies, such as Alexa Fluor 488 goat anti-rabbit (A-11008, Invitrogen, Carlsbad, CA, USA) or Alexa Fluor 594 goat anti-mouse (A-11005, Invitrogen, Carlsbad, CA, USA). 4',6-diamidino-2-phenylindole (DAPI) (Solarbio) was used for nuclear visualization. Images were captured using a KF-BIO digital pathology slide scanner (KF-PRO-005, KFBIO, Ningbo, Zhejiang, China). All experiments were repeated at least in triplicate.

2.9 Western Blotting

Animal tissue samples were homogenized using a tissue homogenizer in radio immunoprecipitation assay (RIPA) lysis buffer (Beyotime, Shanghai, China) containing 0.1% phenylmethylsulfonyl fluoride (PMSF). Cells were lysed using RIPA lysis buffer with 0.1% PMSF. The homogenized cell lysates were sonicated at 30 Hz for 3 seconds, repeated three times. Both cell and animal tissue samples were then centrifuged at 15,000 rpm for 20 minutes at 4 °C, and the supernatant collected for protein analysis. Protein concentrations were determined using a protein quantification kit. Protein samples were prepared with a 5 \times loading buffer and adjusted with PBS to ensure equal loading. Equivalent quantities of protein were resolved via sodium dodecyl sulfate-polyacrylamide gel electrophoresis and then electrophoretically transferred onto polyvinylidene fluoride membranes. After blocking for 2 h with 5% skim milk, the membrane was washed with 1 \times tris buffered saline with tween-20 (TBST) and incubated with primary antibodies overnight at 4 °C. The next day, the membrane was washed with TBST and incubated with the corresponding Horseradish Peroxidase-labeled (HRP-labeled) secondary antibody for 1 h at room temperature. Protein bands were visualized using an electrochemiluminescence detection kit (4AW011, 4A Biotech, Suzhou, China), with the signal captured using a chemiluminescence imaging system. Band intensities were quantified by analyzing grayscale values using ImageJ software (National Institutes of Health, Bethesda, MD, USA). All experiments were repeated at least in triplicate.

2.10 RNA Extraction and Quantitative Reverse Transcription Polymerase Chain Reaction (qRT-PCR)

Total RNA was extracted from tissue or cell samples using a commercially available RNA extraction kit (Beyotime, Shanghai, China) according to the manufacturer's instructions. RNA concentration and purity were assessed using a spectrophotometer (DS-11 FX/FX+, Denovix, Wilmington, DE, USA). Complementary DNA (cDNA) was synthesized from 1 μg of total RNA with a reverse transcription kit (Vazyme, Nanjing, China). Quantitative real-time PCR was conducted on a QuantStudio 5 instrument (Thermo Fisher Scientific, USA) using SYBR Green chemistry. Relative gene expression levels were determined with the comparative threshold cycle (Ct) method, and normalized to

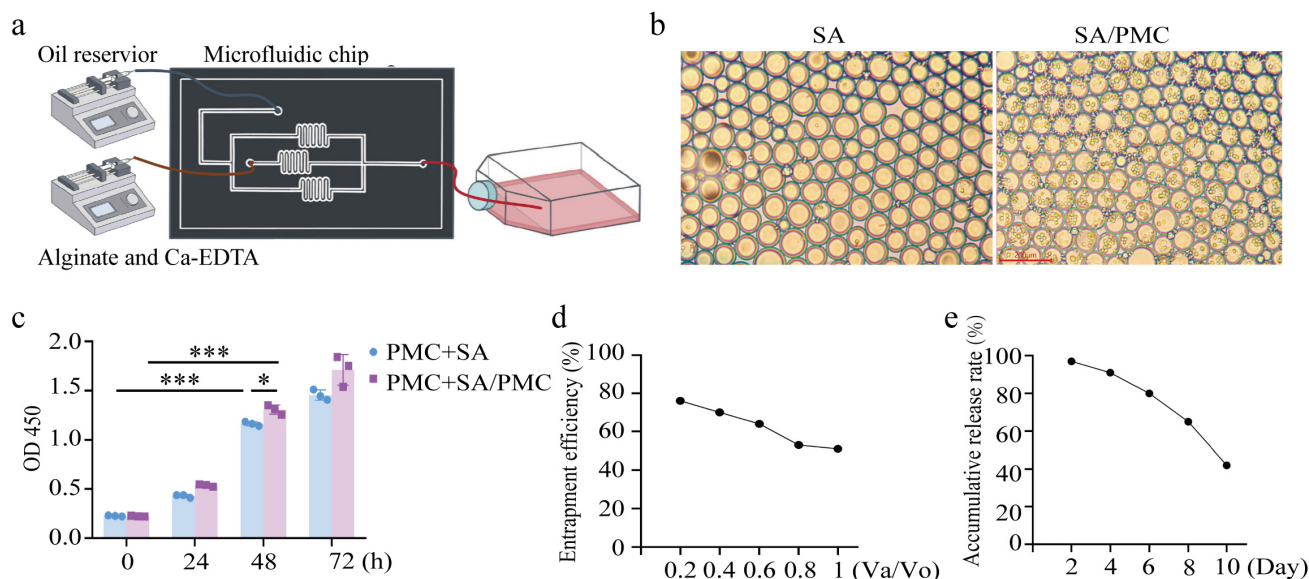


Fig. 1. Characteristic of sodium alginate (SA) microgel. (a) Production of SA microgel. (b) Microstructure of the SA and SA microgels encapsulating peritoneal mesothelial cells (SA/PMCs). Scale bar = 200 μm . (c) Cell counting kit 8 (CCK-8) OD values at 450 nm for primary human peritoneal PMCs co-cultured with SA (PMC+SA), and primary human PMCs co-cultured with SA/PMC (PMC+SA/PMC). (d) Cell encapsulation efficiency under different aqueous and oil phase flow rates (V_a/V_o). (e) Cumulative cell release rate. All data are presented as the mean \pm SD. * $p < 0.05$, *** $p < 0.001$.

glyceraldehyde-3-phosphate dehydrogenase (GAPDH) (internal reference gene). All experiments were repeated at least in triplicate.

2.11 Statistical Analysis

Prism 9 software (GraphPad Software, San Diego, CA, USA) was utilized to generate bar charts and conduct statistical analyses. Data conforming to a normal distribution are expressed as the mean \pm standard deviation, while non-normally distributed data are reported as the median with interquartile range. For the comparison of data between groups, the two independent samples t -test was applied when the variance between groups was homogeneous. A p -value < 0.05 was considered statistically significant.

3. Results

3.1 Characteristics of SA Microgel

The production process for SA microgels is illustrated in Fig. 1a. Optical microscopy revealed the diameter of SA microgels ranged from approximately 60 to 100 μm (Fig. 1b). Encapsulation of PHPMCs within SA (SA/PMC) did not significantly alter the microgel diameter. CCK-8 assays demonstrated a significant increase in PMC proliferation after 48 h of co-culture with both SA and SA/PMC. Moreover, SA/PMC exhibited accelerated cell proliferation compared to the SA-only group (Fig. 1c). As the ratio of the aqueous phase to the oil reservoir flow rate (V_a/V_o) increases, the entrapment efficiency shows a downward trend (Fig. 1d). Meanwhile, with the extension of time, the cumulative release rate gradually rises, reflecting that this hy-

drogel has a certain time dependence in substance release (Fig. 1e). These findings suggest that SA microgels effectively encapsulate PHPMCs and facilitate their release, thereby enhancing cell proliferation.

3.2 Reduced Proliferative Capacity of PHPMCs and Associated EMT in Long-Term PD Patients

Co-staining with cytokeratin 18 (CK18) and vimentin confirmed the identity of cells isolated from PD fluid as PHPMCs (Fig. 2a). PD fluid was collected from patients with PD durations of 1W, 1Y, and 3Y. A high number of PHPMCs was collected in the 1W-PD group, with these cells displayed a cobblestone-like morphology when cultured for 11 days. In contrast, fewer PHPMCs were found in the 1Y-PD group, with the cells undergoing EMT characterized by transition from a cobblestone-like to a spindle-shaped morphology. The 3Y-PD group showed even fewer PHPMCs, with the cells losing their proliferative ability almost entirely (Fig. 2b). These observations indicate that prolonged PD may lead to cell fibrosis and induce EMT.

3.3 Increased Expression of POSTN/NF- κ B/CXCL8 in Long-Term PD Patients With Peritoneal Fibrosis

To investigate the mechanisms underlying peritoneal fibrosis in long-term PD patients, PHPMCs were isolated from PD fluid of patients undergoing dialysis for 1W and 1Y. According to the sequencing results, POSTN and CXCL 8 were increased in patients undergoing peritoneal dialysis for 1 year (Fig. 3a). Immunofluorescence staining indicated a marked upregulation of POSTN expression

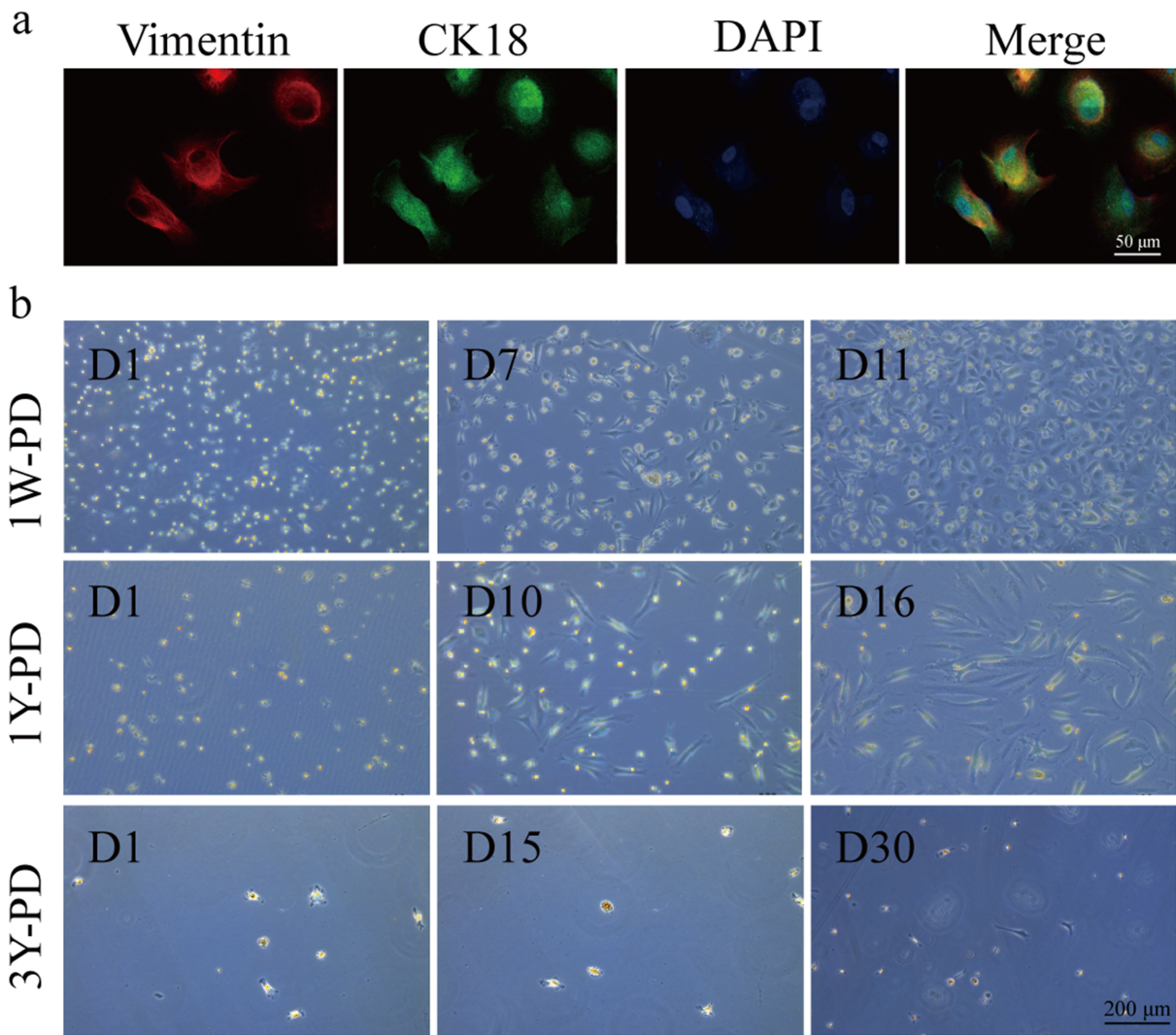


Fig. 2. Reduced proliferative capacity of PHPMCs was associated epithelial-mesenchymal transition in long-term peritoneal dialysis (PD) patients. (a) Representative immunofluorescence images of markers vimentin and cytokeratin 18 (CK18) in PHPMCs. Scale bar = 50 μm. (b) The growing images of PHPMCs of PD patients for 1 week (1W-PD), 1 year (1Y-PD), and 3 year (3Y-PD). Scale bar = 200 μm. D, day.

in the 1Y-PD group relative to the 1W-PD cohort. NF- κ B p65, a downstream target of POSTN, also exhibited increased expression in the 1Y-PD group, as confirmed by immunofluorescence. The activation and nuclear translocation of p-p65 exhibited pronounced nuclear accumulation in the 1Y-PD group. Furthermore, CXCL8, an inflammatory marker associated with peritoneal fibrosis, showed increased protein expression in the 1Y-PD group (Fig. 3d). Importantly, fibrosis-related markers, such as α -SMA, Col-1, TGF- β , and FN also showed elevated protein expression in the 1Y-PD group (Fig. 3b). The same results were confirmed by qRT-PCR and western blots (Fig. 3c–o). Collectively, these findings suggest that in patients undergoing peritoneal dialysis for one year, peritoneal mesothelial cells demonstrate upregulated expression of POSTN, NF- κ B, and CXCL8, along with elevated fibrosis markers.

3.4 SA/PMC Attenuates the High Glucose-Induced Increase in POSTN/NF- κ B/CXCL8 Expression and Fibrosis in PHPMCs

Primary human PMCs were cultured in a 60 mM high glucose medium to examine the role of elevated POSTN expression in fibrosis under high glucose conditions. Immunofluorescence staining revealed increased POSTN expression in the G and G+SA groups, whereas the G+SA/PMC group showed reduced POSTN expression. Similarly, NF- κ B P65 expression was elevated in the G and G+SA groups. High glucose also promoted the phosphorylation and nuclear translocation of P65, thereby increasing CXCL8 expression, but this was inhibited by SA/PMC. Furthermore, elevated expression of fibrosis-related markers (α -SMA, Col-1) was seen in the G and G+SA groups, whereas the G+SA/PMC group

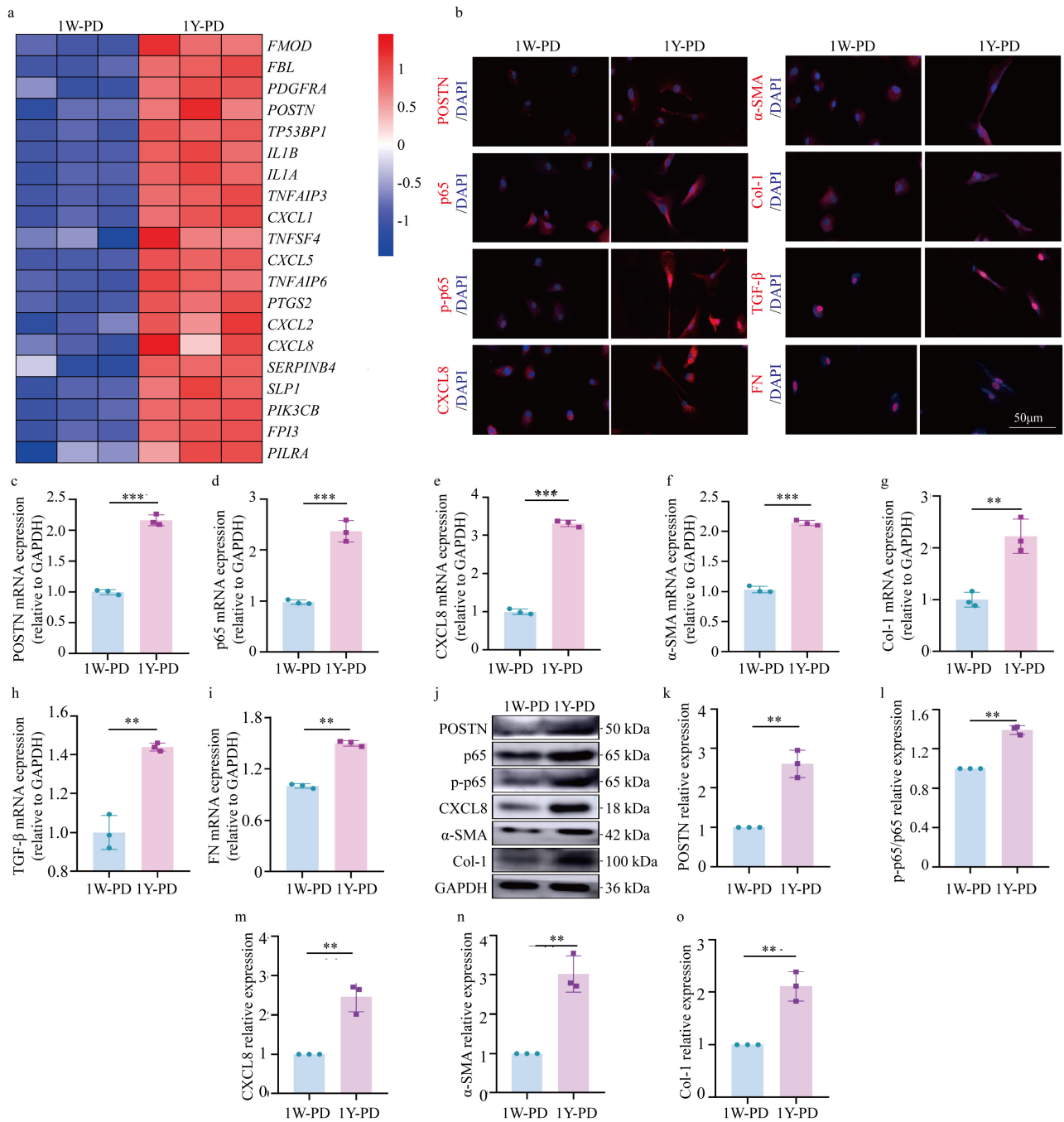


Fig. 3. Increased expression of periostin/nuclear factor kappa-B/C-X-C motif chemokine ligand 8 (POSTN/NF- κ B/CXCL8) in long-term PD patients with peritoneal fibrosis. (a) Heatmap showing differential gene expression in PMCs from 1W-PD and 1Y-PD patients. (b) Representative immunofluorescence images of staining for POSTN, NF- κ B P65, p-P65, CXCL8, α -smooth muscle actin (α -SMA), collagen I (Col-1), transforming growth factor- β (TGF- β), and FN in PMCs from 1W-PD and 1Y-PD patients. Scale bar = 50 μ m. (c–i) mRNA expression levels in the two groups. (j–o) Representative Western blot images and quantitative analysis of POSTN, p-P65/P65, CXCL8, α -SMA, and Col-1 expression in the two groups. All data are presented as the mean \pm SD. ** $p < 0.01$, *** $p < 0.001$.

exhibited reduced levels (Fig. 4a). mRNA analysis confirmed that high glucose increased POSTN/NF- κ B/CXCL8 expression, while SA/PMC treatment reduced the expression of these markers (Fig. 4b–h). Western blot results also demonstrated increased expression levels of POSTN, NF-

κ B P65, and CXCL8 in the G group, with reduced levels in the G+SA/PMC group. The fibrosis marker α -SMA was similarly increased in the G group and decreased in the G+SA/PMC group (Fig. 4i–m). These results demonstrate that high glucose induces POSTN/NF- κ B/CXCL8

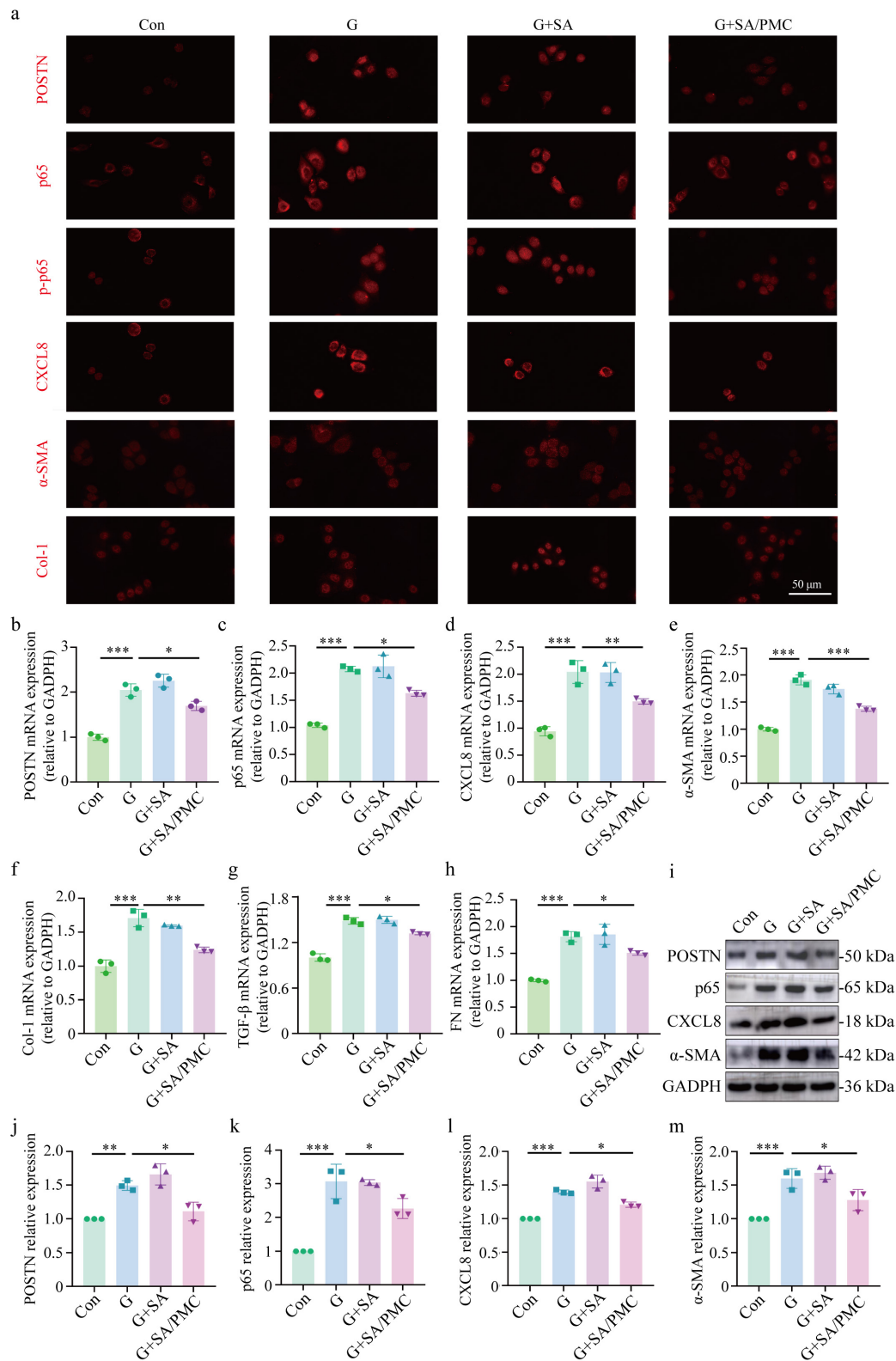


Fig. 4. SA/PMC reduces the high glucose-induced increase in POSTN/NF- κ B/CXCL8 expression and fibrosis in PHPMCs. (a) Representative immunofluorescence images of POSTN, NF- κ B P65, p-P65, CXCL8, α -SMA and Col-1 staining in the Control (Con), high glucose (G), high glucose+SA (G+SA), and high glucose+SA/PMC (G+SA/PMC) groups. Scale bar = 50 μ m. (b–h) mRNA expression level of POSTN, NF- κ B P65, CXCL8, α -SMA, Col-1, TGF- β , and FN in the four groups. (i–m) Representative Western blot images and quantitative analysis of POSTN, NF- κ B P65, CXCL8, and α -SMA in the four groups. All data are presented as the mean \pm SD. * p < 0.05, ** p < 0.01, *** p < 0.001.

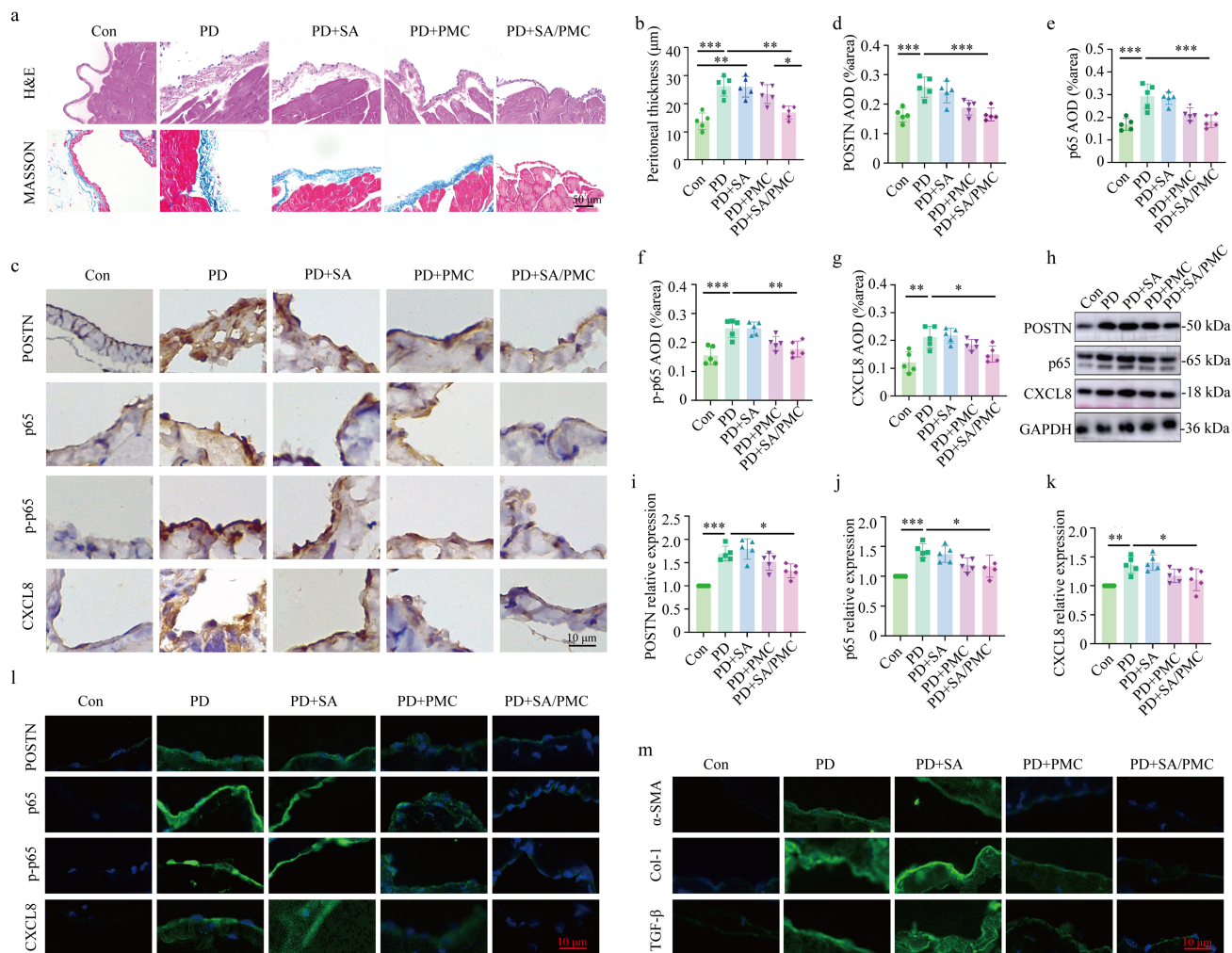


Fig. 5. Increased expression of POSTN/NF- κ B/CXCL8 and marked peritoneal fibrosis in the mouse PD model. (a) Hematoxylin and eosin (H&E) and MASSON staining of parietal peritoneum in the mouse PD model. Scale bar = 50 μ m. (b) Thickness of the parietal peritoneum. (c) Representative immunohistochemical staining for POSTN, NF- κ B P65, p-P65, and CXCL8. Scale bar = 10 μ m. (d–g) Quantitative analysis of the expression of POSTN, NF- κ B P65, p-P65, and CXCL8 shown in (c). (h–k) Representative Western blot images and quantitative analysis of POSTN, NF- κ B P65, and CXCL8 proteins shown in (h). (l) Representative immunofluorescence images of staining for POSTN, NF- κ B P65, p-P65 and CXCL8. Scale bar = 10 μ m. (m) Representative immunofluorescence images of staining for α -SMA, Col-1, and TGF- β . All data are presented as the mean \pm SD. Scale bar = 10 μ m. * p < 0.05, ** p < 0.01, *** p < 0.001.

expression and EMT in PMCs, which can be mitigated by SA/PMC treatment.

3.5 Increased Expression of POSTN/NF- κ B/CXCL8 and Marked Peritoneal Fibrosis in the Mouse PD Model

A murine model of PD was used to further investigate the involvement of POSTN in peritoneal fibrogenesis. MASSON staining indicated significant peritoneal fibrosis in the PD, PD+SA, and PD+PMC groups, whereas the PD+SA/PMC group showed reduced fibrosis (Fig. 5a). Additionally, the peritoneal thickness was significantly greater in the PD and PD+SA groups compared to the control group, but significantly smaller in the PD+SA/PMC group compared to the PD and PD+PMC groups (Fig. 5b). Im-

munochemical assessment indicated elevated POSTN expression in the PD group, which was substantially attenuated in the PD+SA/PMC treatment group. Importantly, POSTN expression in the PD+SA/PMC group was lower than in the PD+PMC group. Similarly, the levels of NF- κ B P65, p-P65, and CXCL8 were elevated in the PD group and reduced in the PD+SA/PMC group (Fig. 5c–g). Western blot analysis corroborated the findings that POSTN, NF- κ B, and CXCL8 protein expression levels were elevated in the PD group, but significantly reduced following PD+SA/PMC treatment, with lower levels in the PD+SA/PMC group compared to the PD+PMC group (Fig. 5h–k). Additionally, immunofluorescence showed increased fluorescence intensity for POSTN, NF- κ B P65,

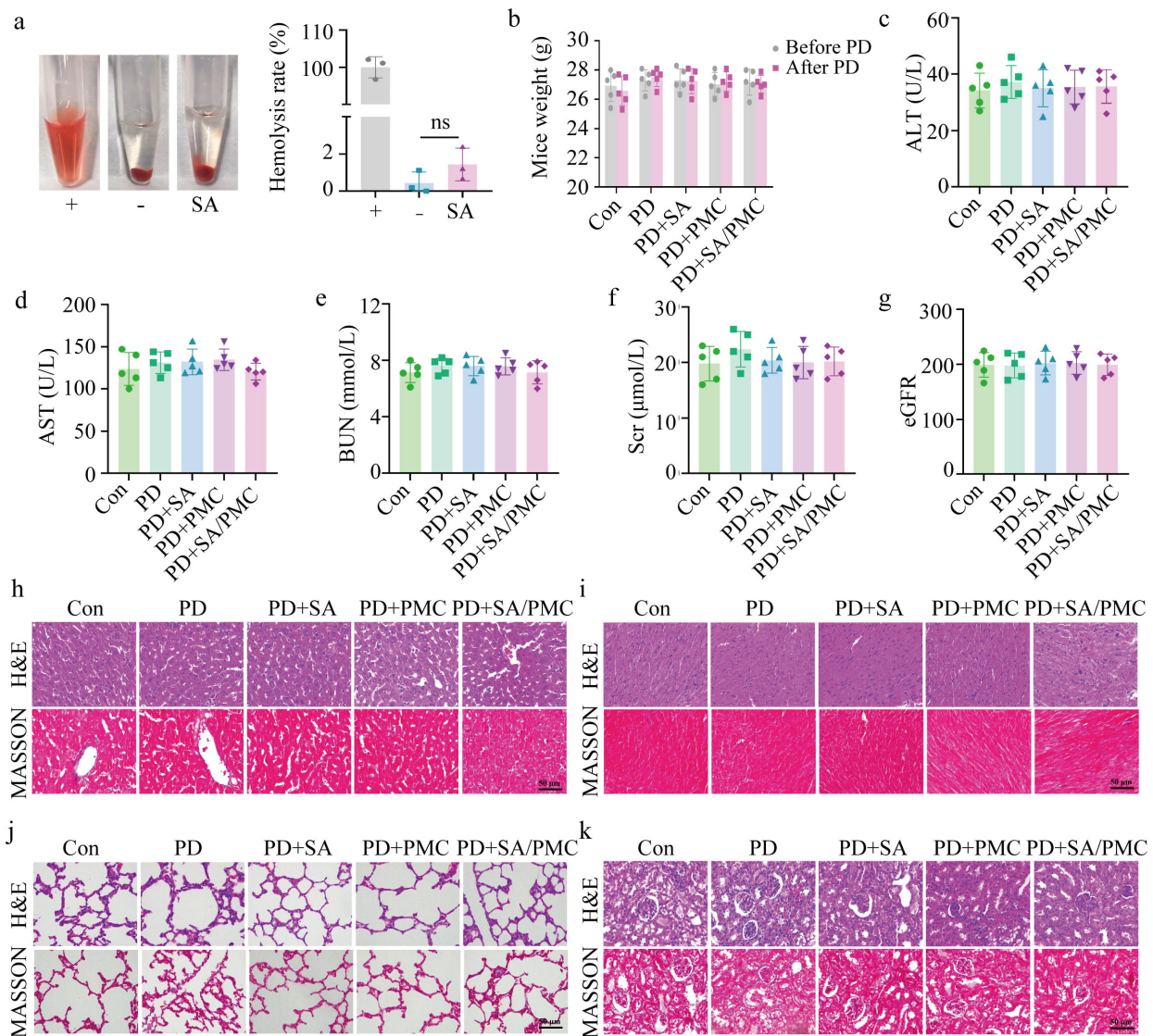


Fig. 6. Biosafety of SA microgels. (a) Images of hemolysis test and hemolysis rate. (b) Body weight of mice before and after PD. (c) Alanine aminotransferase (ALT) level of PD mice. (d) Aspartate aminotransferase (AST) level. (e) Blood urea nitrogen (BUN) level. (f) Serum creatinine (Scr) level. (g) Glomerular filtration rate (eGFR). (h–k) Representative H&E and MASSON images of liver, heart, lung, and kidney. All data are presented as the mean \pm SD. Scale bar = 50 μm . ns, no significant difference.

p-P65, CXCL8, α -SMA, Col-1, and TGF- β in the PD group, which was reduced in the PD+SA/PMC group (Fig. 5l,m). These findings indicate that high glucose PD induces POSTN/NF- κ B/CXCL8 expression and peritoneal fibrosis in mice, with SA/PMC treatment showing superior antifibrotic effects compared to SA.

3.6 In Vivo Biocompatibility of SA Microgels

To evaluate the biosafety of SA microgels, blood and tissue samples were collected from the various groups of PD mice. Hemolysis tests indicated that adding SA to mouse blood resulted in a hemolysis rate of $<2\%$, suggesting good blood compatibility (Fig. 6a,b). Moreover, no significant changes in body weight were observed during the PD period (Fig. 6c). To assess the impact of SA microgel on liver and

kidney function, we measured the levels of alanine aminotransferase (ALT), aspartate aminotransferase (AST), blood urea nitrogen (BUN), serum creatinine (Scr), and glomerular filtration rate (eGFR). None of these parameters showed any significant abnormalities (Fig. 6d–g). Furthermore, histological analyses using H&E and Masson staining revealed no significant abnormalities in liver, heart, lung, and kidney tissues (Fig. 6h–k). Collectively, these findings suggest that SA microgels exert minimal adverse effects on the physiological and histological parameters assessed, indicating their potential safety as a therapeutic modality.

4. Discussion

This study explored the therapeutic efficacy of SA/PMC microgels in attenuating peritoneal fibrosis asso-

ciated with long-term PD. Our findings demonstrated successful encapsulation of PHPMCs in SA microgels, which maintained cell proliferation without significantly altering the microgel diameter. The CCK-8 assay further validated that encapsulated PMCs exhibited improved viability and proliferation, highlighting the suitability of SA microgels as a cell delivery system to support cell growth and survival for peritoneal regeneration.

Peritoneal fibrosis is a significant complication of long-term PD, often resulting from continuous exposure to hypertonic glucose-based dialysis solutions, leading to PMC injury and EMT [18,19]. This pathological process is characterized by increased expression of fibrosis markers such as α -SMA, Col-1, TGF- β , and FN [20]. Our findings align with previous research [21,22] indicating that prolonged PD contributes to PMC damage and EMT, thereby promoting fibrosis. Current anti-fibrotic strategies center on blocking key signaling pathways that drive fibrosis, such as with mTOR inhibitors (e.g., rapamycin) [23] and TGF- β pathway inhibitors [24].

Recent studies have highlighted the role of POSTN, a matricellular protein, in the progression of CKD and its involvement in fibrotic processes [25,26]. POSTN has been shown to mediate kidney disease in response to TGF- β , suggesting that targeting of this ECM protein could be a promising therapeutic strategy to prevent CKD progression [27]. POSTN has also been implicated in activating the ERK and NF- κ B pathways [28,29], leading to the expression of pro-inflammatory cytokines such as CXCL8, which further exacerbate fibrotic responses. In our study, immunofluorescence, PCR sequencing, and Western blot analyses confirmed elevated expression of POSTN, NF- κ B p65, p-p65, and CXCL8 in long-term PD patients. The increased nuclear translocation of p-p65 and the upregulation of fibrosis-related markers such as α -SMA, Col-1, TGF- β , and FN further confirmed activation of the POSTN/NF- κ B/CXCL8 signaling axis in the context of peritoneal fibrosis. These findings are consistent with a previous study demonstrating that POSTN can trigger inflammatory responses through NF- κ B signaling, contributing to fibrotic processes [30].

Our *in vitro* experiments demonstrated that high glucose stimulation of PMCs led to increased POSTN/p65/CXCL8 expression and fibrosis, which were significantly mitigated by SA/PMC treatment. This suggests that SA/PMC microgels can effectively inhibit the high glucose-induced fibrotic response. Similarly, *in vivo* studies with a mouse PD model further supported these findings, with SA/PMC treatment significantly reducing peritoneal fibrosis, as evidenced by decreased expression of POSTN, p65, p-P65, and CXCL8, and reduced thickness of the peritoneal membrane. These results concur with previous reports that targeting POSTN and the NF- κ B signaling pathway can effectively mitigate fibrotic processes. Additionally, biosafety assessments confirmed that

SA microgels did not induce significant adverse effects. Normal liver and kidney function were maintained, and no histological abnormalities were observed in major organs. This highlights the potential of SA/PMC microgels as a safe and effective therapeutic approach for peritoneal fibrosis.

This study has several limitations. A key limitation of this study is the absence of direct functional validation of the POSTN/NF- κ B/CXCL8 signaling pathway, as well as a lack of *in vivo* tracking evidence demonstrating the release and engraftment of encapsulated PHPMCs. Furthermore, the study did not directly compare the observed effects with those of established anti-fibrotic agents like rapamycin or TGF- β inhibitors. Another limitation of this study is the absence of essential control groups, such as SA/PMC treatment under normal glucose conditions and SA/PMC treatment in healthy mice without PD solution. These aspects will be addressed in future studies through targeted inhibition and live-cell tracking assays to confirm mechanistic causality and cellular dynamics.

5. Conclusions

In conclusion, our study suggests that SA/PMC microgels could represent a promising therapeutic strategy for mitigating peritoneal fibrosis in PD patients. By encapsulating PHPMCs and modulating the POSTN/NF- κ B/CXCL8 pathway, we hypothesize that these microgels gradually release PHPMCs, potentially replacing damaged cells, inhibiting EMT, and alleviating peritoneal fibrosis. However, additional studies, including *in vivo* tracking of PHPMCs, are required to confirm the release dynamics, cell survival, migration, and integration into the peritoneum. Future research should prioritize clinical trials to further validate these findings and assess the long-term safety and efficacy of SA/PMC microgels in PD patients.

Availability of Data and Materials

Data are available from the corresponding author on reasonable request.

Author Contributions

SM, XY, CS, ChuZ and YZ conceived and designed the study. SM, CQ, JuZ, ZL, LW, YY, CS, YW and CC performed the experiments and collected the data. SM, CQ, JuZ, KZ, CheZ, YB and YS analyzed and interpreted the data. All authors critically reviewed and contributed to manuscript revisions, read and approved the final version, fully participated in the work, and agree to be accountable for all aspects of the study.

Ethics Approval and Consent to Participate

The study was conducted in accordance with the Declaration of Helsinki, and the protocol was approved by the Human Ethics Committee of Wenzhou Medical Univer-

sity (Acceptance number: KY2024-R179). All participants provided written informed consent prior to their inclusion in the study. The animal-study protocol was reviewed and approved by the Wenzhou Medical University Laboratory Animal Ethics Committee (approval No. WYYY-AEC-YS-2024-0547). All animal procedures strictly adhered to the relevant institutional, national, and international guidelines, including the revised Animals (Scientific Procedures) Act 1986 (UK) and Directive 2010/63/EU (EU).

Acknowledgment

We would like to express our sincere gratitude to all the members of the laboratory for their invaluable assistance and insightful discussions throughout this research.

Funding

This research was funded by Zhejiang Province Natural Science Foundation, grant number LTGY23H050003 and LTGY24H050004 and Wenzhou Committee of Science and Technology of China, grant number Y2023065.

Conflict of Interest

The authors declare no conflict of interest.

Declaration of AI and AI-Assisted Technologies in the Writing Process

During the preparation of this work the authors used ChatGpt in order to check spell and grammar. After using this tool, the authors reviewed and edited the content as needed and takes full responsibility for the content of the publication.

References

- [1] Bello AK, Okpechi IG, Osman MA, Cho Y, Cullis B, Htay H, *et al.* Epidemiology of peritoneal dialysis outcomes. *Nature Reviews. Nephrology.* 2022; 18: 779–793. <https://doi.org/10.1038/s41581-022-00623-7>.
- [2] Jiang N, Zhang Q, Chau MK, Yip MS, Lui SL, Liu S, *et al.* Anti-fibrotic effect of decorin in peritoneal dialysis and PD-associated peritonitis. *EBioMedicine.* 2020; 52: 102661. <https://doi.org/10.1016/j.ebiom.2020.102661>.
- [3] Yu F, Chen J, Wang X, Hou S, Li H, Yao Y, *et al.* Metabolic reprogramming of peritoneal mesothelial cells in peritoneal dialysis-associated fibrosis: therapeutic targets and strategies. *Cell Communication and Signaling: CCS.* 2025; 23: 114. <https://doi.org/10.1186/s12964-025-02113-2>.
- [4] Hu W, Li G, Dong W, He P, Liu W, Wu Y, *et al.* Single-cell sequencing reveals peritoneal environment and insights into fibrosis in CAPD patients. *iScience.* 2023; 26: 106336. <https://doi.org/10.1016/j.isci.2023.106336>.
- [5] Masola V, Bonomini M, Borrelli S, Di Liberato L, Vecchi L, Onisto M, *et al.* Fibrosis of Peritoneal Membrane as Target of New Therapies in Peritoneal Dialysis. *International Journal of Molecular Sciences.* 2022; 23: 4831. <https://doi.org/10.3390/ijms23094831>.
- [6] Mo M, Zeng Y, Zeng Y, Li S, He X, Chen X, *et al.* N-methylpiperazine-diepoxyvatodiolide ameliorates peritoneal fibrosis via suppressing TGF- β /Smad and JAK/STAT signaling pathway. *Chemico-biological Interactions.* 2023; 382: 110589. <https://doi.org/10.1016/j.cbi.2023.110589>.
- [7] Terri M, Trionfetti F, Montaldo C, Cordani M, Tripodi M, Lopez-Cabrera M, *et al.* Mechanisms of Peritoneal Fibrosis: Focus on Immune Cells-Peritoneal Stroma Interactions. *Frontiers in Immunology.* 2021; 12: 607204. <https://doi.org/10.3389/fimmu.2021.607204>.
- [8] Su W, Hu Z, Zhong X, Cong A, Zhang Y, Zhou Z, *et al.* Restoration of CPT1A-mediated fatty acid oxidation in mesothelial cells protects against peritoneal fibrosis. *Theranostics.* 2023; 13: 4482–4496. <https://doi.org/10.7150/thno.84921>.
- [9] Zheng L, Chen W, Yao K, Xie Y, Liao C, Zhou T. Clinical and preclinical studies of mesenchymal stem cells to alleviate peritoneal fibrosis. *Stem Cell Research & Therapy.* 2024; 15: 237. <https://doi.org/10.1186/s13287-024-03849-3>.
- [10] Jiang S, Jing H, Zhuang Y, Cui J, Fu Z, Li D, *et al.* BMSCs-laden mechanically reinforced bioactive sodium alginate composite hydrogel microspheres for minimally invasive bone repair. *Carbohydrate Polymers.* 2024; 332: 121933. <https://doi.org/10.1016/j.carbpol.2024.121933>.
- [11] Dubay R, Urban JN, Darling EM. Single-Cell Microgels for Diagnostics and Therapeutics. *Advanced Functional Materials.* 2021; 31: 2009946. <https://doi.org/10.1002/adfm.202009946>.
- [12] Ahn SH, Rath M, Tsao CY, Bentley WE, Raghavan SR. Single-Step Synthesis of Alginate Microgels Enveloped with a Covalent Polymeric Shell: A Simple Way to Protect Encapsulated Cells. *ACS Applied Materials & Interfaces.* 2021; 13: 18432–18442. <https://doi.org/10.1021/acsami.0c20613>.
- [13] Bochenek MA, Veiseh O, Vegas AJ, McGarrigle JJ, Qi M, Marchese E, *et al.* Alginate encapsulation as long-term immune protection of allogeneic pancreatic islet cells transplanted into the omental bursa of macaques. *Nature Biomedical Engineering.* 2018; 2: 810–821. <https://doi.org/10.1038/s41551-018-0275-1>.
- [14] Dhawan A, Chaijitraruch N, Fitzpatrick E, Bansal S, Filippi C, Lehec SC, *et al.* Alginate microencapsulated human hepatocytes for the treatment of acute liver failure in children. *Journal of Hepatology.* 2020; 72: 877–884. <https://doi.org/10.1016/j.jhep.2019.12.002>.
- [15] Li Y, Cheng S, Wen H, Xiao L, Deng Z, Huang J, *et al.* Coaxial 3D printing of hierarchical structured hydrogel scaffolds for on-demand repair of spinal cord injury. *Acta Biomaterialia.* 2023; 168: 400–415. <https://doi.org/10.1016/j.actbio.2023.07.020>.
- [16] An C, Liu W, Zhang Y, Pang B, Liu H, Zhang Y, *et al.* Continuous microfluidic encapsulation of single mesenchymal stem cells using alginate microgels as injectable fillers for bone regeneration. *Acta Biomaterialia.* 2020; 111: 181–196. <https://doi.org/10.1016/j.actbio.2020.05.024>.
- [17] Hu Y, Azadi G, Ardekani AM. Microfluidic fabrication of shape-tunable alginate microgels: effect of size and impact velocity. *Carbohydrate Polymers.* 2015; 120: 38–45. <https://doi.org/10.1016/j.carbpol.2014.11.053>.
- [18] Huang Y, Ma J, Fan Y, Yang L. Mechanisms of human umbilical cord mesenchymal stem cells-derived exosomal lncRNA GAS5 in alleviating EMT of HPMCs via Wnt/ β -catenin signaling pathway. *Aging.* 2023; 15: 4144–4158. <https://doi.org/10.18632/aging.204719>.
- [19] Huang Q, Sun Y, Peng L, Sun J, Sha Z, Lin H, *et al.* Extracellular vesicle-packaged ILK from mesothelial cells promotes fibroblast activation in peritoneal fibrosis. *Journal of Extracellular Vesicles.* 2023; 12: e12334. <https://doi.org/10.1002/jev2.12334>.
- [20] Wang Y, Zhang Y, Ma M, Zhuang X, Lu Y, Miao L, *et al.* Mechanisms underlying the involvement of peritoneal macrophages in the pathogenesis and novel therapeutic strategies for dialysis-induced peritoneal fibrosis. *Frontiers in Immunology.* 2024; 15: 1507265. <https://doi.org/10.3389/fimmu.2024.1507265>.
- [21] Jiao T, Huang Y, Sun H, Yang L. Exosomal lnc-CDHR derived from human umbilical cord mesenchymal stem cells at-

- tenuates peritoneal epithelial-mesenchymal transition through AKT/FOXO pathway. *Aging*. 2023; 15: 6921–6932. <https://doi.org/10.18632/aging.204883>.
- [22] Kidney Disease: Improving Global Outcomes (KDIGO) CKD Work Group. KDIGO 2024 Clinical Practice Guideline for the Evaluation and Management of Chronic Kidney Disease. *Kidney International*. 2024; 105: S117–S314. <https://doi.org/10.1016/j.kint.2023.10.018>.
- [23] Jia M, Qiu H, Lin L, Zhang S, Li D, Jin D. Inhibition of PI3K/AKT/mTOR Signalling Pathway Activates Autophagy and Suppresses Peritoneal Fibrosis in the Process of Peritoneal Dialysis. *Frontiers in Physiology*. 2022; 13: 778479. <https://doi.org/10.3389/fphys.2022.778479>.
- [24] Patel P, Sekiguchi Y, Oh KH, Patterson SE, Kolb MRJ, Margetts PJ. Smad3-dependent and -independent pathways are involved in peritoneal membrane injury. *Kidney International*. 2010; 77: 319–328. <https://doi.org/10.1038/ki.2009.436>.
- [25] Pană N, Căpușă C. Periostin as a Biomarker in the Setting of Glomerular Diseases-A Review of the Current Literature. *Biomedicines*. 2022; 10: 3211. <https://doi.org/10.3390/biomedicines10123211>.
- [26] Jia YY, Yu Y, Li HJ. The research status and prospect of Periostin in chronic kidney disease. *Renal Failure*. 2020; 42: 1166–1172. <https://doi.org/10.1080/0886022X.2020.1846562>.
- [27] Cho A, Jin W, Lee J, Shin N, Lee MS, Li L, *et al*. Periostin deficiency attenuates kidney fibrosis in diabetic nephropathy by improving pancreatic β -cell dysfunction and reducing kidney EMT. *Scientific Reports*. 2023; 13: 17599. <https://doi.org/10.1038/s41598-023-44177-5>.
- [28] Lin SC, Liao YC, Chen PM, Yang YY, Wang YH, Tung SL, *et al*. Periostin promotes ovarian cancer metastasis by enhancing M2 macrophages and cancer-associated fibroblasts via integrin-mediated NF- κ B and TGF- β 2 signaling. *Journal of Biomedical Science*. 2022; 29: 109. <https://doi.org/10.1186/s12929-022-00888-x>.
- [29] Zhang Y, Liang J, Cao N, Gao J, Song L, Tang X. Coal dust nanoparticles induced pulmonary fibrosis by promoting inflammation and epithelial-mesenchymal transition via the NF- κ B/NLRP3 pathway driven by IGF1/ROS-mediated AKT/GSK3 β signals. *Cell Death Discovery*. 2022; 8: 500. <https://doi.org/10.1038/s41420-022-01291-z>.
- [30] Abbad L, Prakoura N, Michon A, Chalghoumi R, Reichelt-Wurm S, Banas MC, *et al*. Role of Periostin and Nuclear Factor- κ B Interplay in the Development of Diabetic Nephropathy. *Cells*. 2022; 11: 2212. <https://doi.org/10.3390/cells11142212>.